

# Isotope effects in the dissociation of the $\tilde{B}^1A_1$ state of SiH<sub>2</sub>, SiHD, and SiD<sub>2</sub> using three-dimensional wave packet propagation

Ikuo Tokue<sup>a)</sup> and Katsuyoshi Yamasaki<sup>b)</sup>*Department of Chemistry, Faculty of Science, Niigata University, Ikarashi, Niigata 950-2181, Japan*Shinkoh Nanbu<sup>c)</sup>*Computer Center, Institute for Molecular Science, Myodaiji, Okazaki 444-8585, Japan*

(Received 20 December 2005; accepted 9 February 2006; published online 20 March 2006)

Dissociations after the  $\tilde{A}^1B_1 \rightarrow \tilde{B}^1A_1$  photoexcitation of SiH<sub>2</sub>, SiHD, and SiD<sub>2</sub> were studied to investigate excited-state dynamics and effects of the initial vibrational state. The cross section ( $\sigma$ ) for the photodissociation relative to SiH<sub>2</sub>( $\tilde{B}$ )  $\rightarrow$  Si(<sup>1</sup>D)+H<sub>2</sub> and the rovibrational population of the H<sub>2</sub> fragment were computed using the wave packet propagation technique based on the three-dimensional potential energy surfaces (PESs) of the  $\tilde{A}$  and  $\tilde{B}$  electronic states and the transition dipole surfaces, which were reported in our previous paper [J. Chem. Phys. **122**, 144307 (2005)]. The photodissociation spectrum consists of a broadband and a number of sharp peaks. For SiH<sub>2</sub> and SiD<sub>2</sub>, the sharp peaks correspond to the resonance structure of the vibrational levels of the  $\tilde{B}$  state and the broadbands are nearly independent of the photon energy. The broadband for SiHD increases steeply with the photon energy above 30 000 cm<sup>-1</sup>. The flux leaving the computational grid for SiH<sub>2</sub> and SiD<sub>2</sub> consists of at least two components, whereas that for SiHD consists of only a faster component. These large isotope effects were discussed based on the valley to the dissociation channel on PES and the difference in the position of the initial wave packet for three isotopomers. © 2006 American Institute of Physics. [DOI: 10.1063/1.2183301]

## I. INTRODUCTION

Silicon dihydride SiH<sub>2</sub> appears as an important intermediate during decomposition reactions of silane, which have attracted much attention because of their importance in manufacturing amorphous silicon. SiH<sub>2</sub> can undergo further dissociation SiH+H or Si+H<sub>2</sub>. The dissociation processes of the low-lying electronic states of SiH<sub>2</sub> have been studied experimentally and theoretically.<sup>1-7</sup> The predissociation of the  $\tilde{A}^1B_1$  state to Si(<sup>3</sup>P)+H<sub>2</sub> via the  $\tilde{a}^3B_1$  state has been known to depend strongly on the rotational levels. The next higher channel is the dissociation to Si(<sup>1</sup>D)+H<sub>2</sub>. The onset of the Si(<sup>1</sup>D)+H<sub>2</sub> channel appears to open between the (0,6,0) and (0,7,0) levels of the  $\tilde{A}$  state.<sup>2,5</sup> Recently, Muramoto *et al.* studied the  $\tilde{B}^1A_1$  state of SiH<sub>2</sub> and SiD<sub>2</sub> by the optical-optical double resonance technique.<sup>8</sup> The predissociation rate was observed to increase with the vibrational energy. In addition, the linewidths of SiD<sub>2</sub> were found to be narrower than those of SiH<sub>2</sub> indicating that the dissociation rates of SiH<sub>2</sub> are faster than those of SiD<sub>2</sub>. Although dissociation dynamics of the  $\tilde{B}$  state should be reflected in these observations, we did not find any theoretical information.

In the preceding paper,<sup>9</sup> we reported *ab initio* molecular

orbital configuration interaction (MOCI) calculations used in our determination of the global potential energy surfaces (PESs) for the  $\tilde{X}^1A_1$ ,  $\tilde{A}^1B_1$ , and  $\tilde{B}^1A_1$  states, quantum vibrational calculations used to obtain vibrational levels for each electronic state of SiH<sub>2</sub> and SiD<sub>2</sub>, as well as calculations of the Franck-Condon factors (FCFs) and the transition probabilities used to obtain the vibrational distribution in the photoabsorption. The main purpose of this paper is to elucidate the dissociation mechanism of SiH<sub>2</sub>( $\tilde{B}^1A_1$ )  $\rightarrow$  Si(<sup>1</sup>D)+H<sub>2</sub> induced by the  $\tilde{A} \rightarrow \tilde{B}$  photoexcitation especially paying attention to effects of excited-state dynamics and the initial vibrational state. The H<sub>2</sub> fragment from SiH<sub>2</sub>( $\tilde{B}$ ) seems to be rotationally excited since the equilibrium bond angle of the  $\tilde{B}$  state is very larger than that of the  $\tilde{A}$  state. Therefore full three-dimensional calculations should be required for the SiH<sub>2</sub>( $\tilde{B}$ ) system. Section II outlines wave packet dynamics used to obtain the photodissociation cross sections and the rovibrational distributions of the H<sub>2</sub> fragment. Section III summarizes theoretical results and discusses the photodissociation dynamics of the  $\tilde{B}$  state of SiH<sub>2</sub>, SiHD, and SiD<sub>2</sub>.

## II. THEORETICAL METHODS

### A. *Ab initio* MOCI and quantum vibrational calculations

Details in the calculations of PESs and vibrational energies were reported in the preceding paper.<sup>9</sup> Briefly, the basis set was the diffusion-function-augmented correlation consistent, polarized valence, quadruple zeta (aug-cc-pVQZ) of

<sup>a)</sup> Author to whom correspondence should be addressed. Fax: +81-25262-6116. Electronic mail: itok-pc@chem.sc.niigata-u.ac.jp

<sup>b)</sup> Present address: Department of Chemistry, Hiroshima University, Hiroshima, Japan.

<sup>c)</sup> Present address: Computing and Communications Center, Kyushu University, Fukuoka, Japan.

Woon and Dunning,<sup>10</sup> and the molecular orbitals were determined by complete active space self-consistent calculations. After determining the MOs, multireference configuration interaction calculations were carried out. The two lowest  $\tilde{X}^1A_1$  and  $\tilde{A}^1B_1$  states are derived from  $^1\Pi_u$  from the Renner-Teller (RT) interaction, and correlate with the  $H_2(X^1\Sigma^+) + Si(^1D_g)$  system in the dissociation limit. The  $\tilde{B}^1A_1$  state correlates with the same  $H_2(X^1\Sigma^+) + Si(^1D_g)$  system. Moreover, the  $\tilde{X}$  and  $\tilde{A}$  states correlate with the  $SiH(X^2\Pi) + H(^2S)$  channel, which is 1.7 eV higher than the  $H_2(X^1\Sigma^+) + Si(^1D_g)$  channel, whereas the  $\tilde{B}$  state correlates with the  $SiH(A^2\Delta) + H(^2S)$  channel. The potential energies for the electronic ground state  $1^1A'$  and the next two electronic excited states  $1^1A''$  and  $2^1A'$  were finally obtained in the  $C_s$  symmetry. The transition dipole moment between the  $\tilde{A}$  and  $\tilde{B}$  states was also evaluated from the CI wave functions. Jacobi coordinates were employed to describe the relative positions of the three nuclei in the body fixed plane;  $r$  is the distance between the two H atoms,  $R$  is the distance between the Si atom and the center of mass of two H atoms, and  $\theta$  is the angle between the vectors  $\mathbf{R}$  and  $\mathbf{r}$ .

We performed a quantum vibrational calculation based on the discrete variable representations.<sup>11-14</sup> The Hamiltonian matrix and associated wave functions are represented with evenly spaced grids in  $R$  and  $r$ , and associated Legendre polynomials to describe  $\cos \theta$ . The grid parameters were suitable for the radial part: ( $N_R=167$ ,  $R_{\min}=0.0a_0$ , and  $R_{\max}=12.0a_0$ ) and ( $N_r=119$ ,  $r_{\min}=1.0a_0$ , and  $r_{\max}=10.0a_0$ ), where  $N$  is the number of grid points and  $a_0$  is the Bohr radius. The number of Legendre functions was 60 for the angular part. The method adopted for the diagonalization of the Hamiltonian matrix is the implicitly restricted Lanczos method.<sup>15</sup> In the present work, assuming the total angular momentum  $J=0$  and 1, the lowest 80 vibrational states were obtained for the three electronic states of  $SiH_2$ ,  $SiHD$ , and  $SiD_2$ .

## B. Wave packet dynamics

The wave packet propagation technique used in the present work was the “real wave packet” method.<sup>16</sup> The wave packet is represented using evenly spaced grids in  $R$  and  $r$  and a Legendre basis set in  $\cos(\theta)$ . The absorption potential used in the real wave packet propagation is taken as

$$A(x) = \exp[-C_{\text{abs}}(x - x_{\text{abs}})^2] \quad \text{for } x > x_{\text{abs}}, \quad (1)$$

where  $x=R$ ,  $x_{\text{abs}}=7.0a_0$ , and  $C_{\text{abs}}=0.25$ , and where  $x=r$ ,  $x_{\text{abs}}=6.0a_0$ , and  $C_{\text{abs}}=0.25$ .

To simulate the dissociation process induced by the  $\tilde{A} \rightarrow \tilde{B}$  photoexcitation, one must determine the initial wave packet correctly. In the time-dependent formulation, the product of the transition dipole moment function with the  $\tilde{A}$  state initial vibrational function gives the initial wave function,<sup>17</sup>

$$\Phi_{\text{init}}(R, r, \theta, t=0) = \mu(R, r, \theta) \Psi_A(R, r, \theta), \quad (2)$$

where  $\mu(R, r, \theta)$  is the transition dipole moment function for

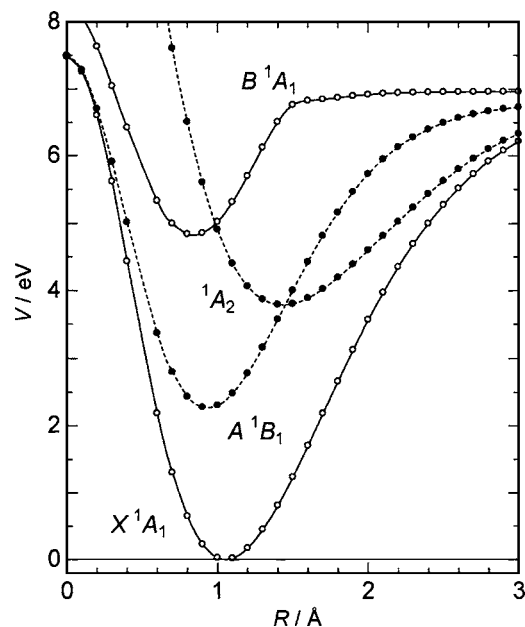


FIG. 1. Potential energies for the four lowest states in eV as a function of  $R$ ;  $r$  is fixed at the equilibrium length of 2.19 Å for the ground state and  $\theta = 90^\circ$ .

the  $\tilde{A}-\tilde{B}$  system, and  $\Psi_A(R, r, \theta)$  is the initial vibrational wave function of the  $\tilde{A}$  state. The resulting wave function  $\Phi_{\text{init}}(R, r, \theta; t=0)$  is propagated on the PES of the  $\tilde{B}$  state. Therefore, we have calculated the vibrational wave functions of the  $\tilde{A}$  state using a Hamiltonian matrix similar to that of the wave packet propagation; the PES was switched with that of the  $\tilde{B}$  state and the implicitly restarted Lanczos method in ARPACK (Ref. 15) was used to diagonalize the matrix. According to the Lanczos method, one acts repeatedly with the Hamiltonian on the vector, for example, that for wave packet propagation. This method has been shown to be an efficient way of computing a few eigenvalues and corresponding eigenvectors of general large sparse matrices.

After determining the initial wave packet, it was evolved with time on the PES of the  $\tilde{B}$  state, and finally the autocorrelation function was computed by numerically integrating the product of the initial wave packet and the evolving wave packet at each time step. Total photodissociation cross section as a function of the excitation energy was calculated as the Fourier transform of the autocorrelation function as a function of time,<sup>18</sup>

$$\sigma(\nu) = \frac{1}{\pi \sin \theta} \sum_{k=0}^{\infty} (2 - \delta_{k0}) \cos(k\theta) C_k, \quad (3)$$

where  $C_k$  is the order-dependent autocorrelation function in the Chebyshev order domain. In the present work, photodissociation cross sections were computed assuming the total angular momentum  $J=0$  and 1.

TABLE I. Calculated and observed vibronic energies in cm<sup>-1</sup> for the  $\tilde{X}^1A_1$ ,  $\tilde{A}^1B_1$ , and  $\tilde{B}^1A_1$  states of SiHD; the Si-H stretching  $\nu_1$ , bending  $\nu_2$ , and Si-D stretching  $\nu_3$  modes.

$(\nu_1, \nu_2, \nu_3)$	$\tilde{X}^1A_1$			$\tilde{A}^1B_1$	$\tilde{B}^1A_1$	
	Present	$J=0$ Expt. <sup>a</sup>	Theor. <sup>b</sup>	$J=0$ Present <sup>c</sup>	$J=0$	$J=K=1$ Present <sup>d</sup>
(0,0,0)	0		0	15 397	26 997	
(0,1,0)	864	854.3	875	16 224		27 459
(0,2,0)	1712		1758	17 030	27 920	
(0,3,0)	2552		2651	17 830		28 382
(0,4,0)	3383		3553	18 615	28 865	
(0,5,0)	4205		4465	19 384		29 327
(0,6,0)	5018		5385	20 137	29 837	
(0,7,0)	5827		6315	20 717		30 299
(0,8,0)	6637		7254	21 323	30 836	
(0,9,0)	7447		8202	21 925		31 298
(0,10,0)	8252			22 565	31 859	
(0,11,0)	9053			23 248		32 321
(0,12,0)	9848				32 900	
(0,0,1)	1450	1440.0	1474	16 933	28 533	
(0,1,1)	2304		2341	17 738		28 995
(0,2,1)	3142		3218	18 528	29 465	
(0,3,1)	3974		4103	19 302		29 927
(0,4,1)	4798		4998	20 042	30 413	
(0,5,1)	5612			20 876		30 875
(0,6,1)	6420			21 598	31 381	
(0,7,1)	7223			22 307		31 843
(0,8,1)	8025			22 803	32 373	
(1,0,0)	1993	1973.3	2040	17 517	29 107	
(0,0,2)	2860		2914	18 396	29 991	
(1,0,1)	3440		3516	19 027	30 620	
(2,0,0)	3912		4013	19 501	31 099	

<sup>a</sup>Reference 19.<sup>b</sup>Calculated from vibrational constants given by Gabriel *et al.* (Ref. 20).<sup>c</sup>The  $T_e$  value for the  $\tilde{A}$  state is 15 400 cm<sup>-1</sup>, which was subtracted 100 cm<sup>-1</sup> from the calculated value.<sup>d</sup> $\nu_2 = 2\nu_2^{\text{bent}} + K$ .

### III. RESULTS AND DISCUSSION

#### A. Vibronic energies of SiHD

The  $\tilde{A}^1B_1$  state exhibits a conical intersection with the  $^1A_2$  state around  $R=1.4$  Å,  $r=2.19$  Å, and 3.8 eV above the  $\tilde{X}$  state minimum. Figure 1 shows the potential energy curves for the four lowest states in SiH<sub>2</sub>. Since there is considerable mixing between the diabatic state in a region around the intersection region, vibronic energies with  $J=0$  and 1 were calculated up to 9000 cm<sup>-1</sup> from the potential minimum of the  $\tilde{A}$  state. Those energies for the  $\tilde{B}$  state were calculated up to 8000 cm<sup>-1</sup> for three isotopomers to analyze the vibrational structures of the  $\tilde{A} \rightarrow \tilde{B}$  absorption spectra. The vibronic energies for the SiH<sub>2</sub> and SiD<sub>2</sub> were reported in the preceding paper.<sup>9</sup> For  $\tilde{X}$  and  $\tilde{B}$  states of SiHD, the vibrational quantum numbers ( $\nu_1, \nu_2, \nu_3$ ) have been assigned up to 80 levels. The linear notation of bending vibrational quantum states was applied to the bending modes ( $\nu_2$ ) for the  $\tilde{B}$  state because of a quasilinear geometry. The vibrational levels especially the higher bending levels for the  $\tilde{A}$  state show strong coupling compared to those for the  $\tilde{X}$  state. Therefore we cannot

assign above the 80th level for the  $\tilde{A}$  state because of mixing.

Table I summarizes the vibronic energies for the  $\tilde{X}$  and  $\tilde{A}$  states with  $J=0$  and for the  $\tilde{B}$  state with  $J=0$  and 1 ( $K=1$ ) of SiHD compared with data obtained by the experiment<sup>19</sup> and the other theoretical study.<sup>20</sup> Although there is not enough of the observed vibrational levels to compare the energy with the present data, the accuracy of the vibronic energies for all the states is estimated to be sufficient up to the (0, 12, 0) level in this calculation based on the comparison of the calculated energies with the observed SiH<sub>2</sub> and SiD<sub>2</sub>.<sup>9</sup> When  $J=0$ , the RT coupling is rigorously neglected, whereas the RT interaction between the  $\tilde{X}$  and  $\tilde{A}$  states should be included in the vibrational levels with  $J>0$  in the rigorous treatment of the vibrational energy and the transition probability. Although the RT effect is small for low bending states, the effect cannot be neglected with increasing the quantum number for the bending mode. Nevertheless, we neglected the RT effect in the calculation for the  $J=1$  state since the difference between the vibronic energy neglected the RT effect and the observed does not seem to increase above the (0, 4, 0) state for SiH<sub>2</sub>.<sup>9</sup>

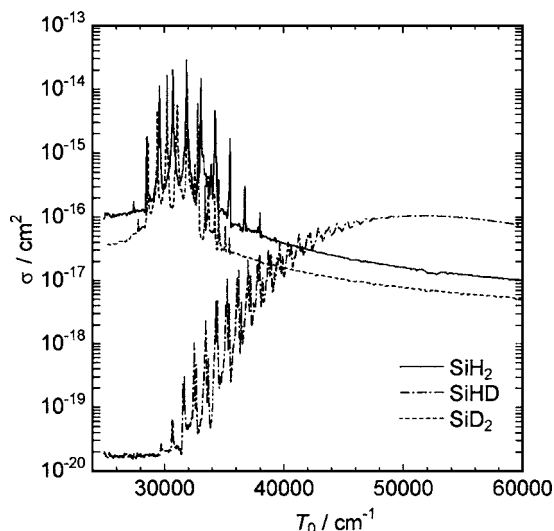


FIG. 2. Theoretical photodissociation spectra for SiH<sub>2</sub>, SiHD, and SiD<sub>2</sub>;  $T_0$  means the excitation energy from the vibrational ground level of the  $\tilde{X}$  state. The initial wave packet is for the (0,0,0) level with  $J=0$  of the  $\tilde{A}$  state.

### B. Photodissociation cross sections

The dissociation of the  $\tilde{B}$  state to the H<sub>2</sub>( $X^1\Sigma^+$ ) + Si( $^1D_g$ ) system is 0.78 eV exothermic in this calculation. The barrier height of the transition state is evaluated to be 3.03 eV from the local minimum of the  $\tilde{B}$  state. The next higher dissociation channel to SiH( $A^2\Delta$ ) + H( $^2S$ ) is estimated to be 4.7 eV higher than the H<sub>2</sub> + Si( $^1D$ ) system. Therefore,

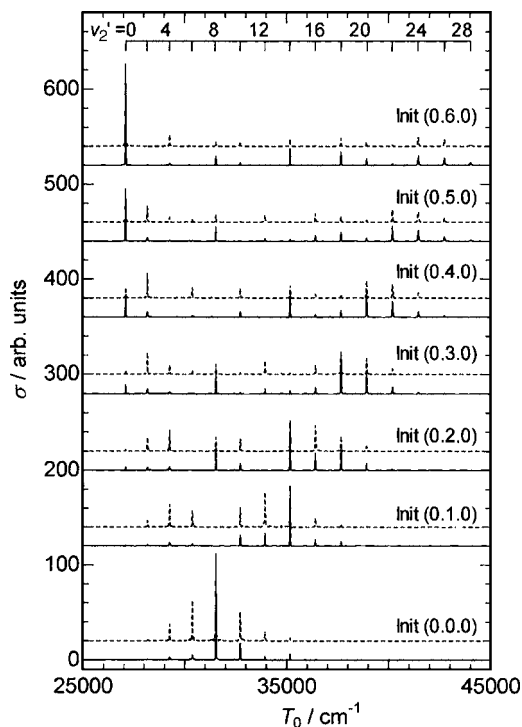


FIG. 3. Dependence of the  $\sigma$  value on the initial vibrational level (0,  $v_2'$ , 0) with  $J=0$  in the  $\tilde{A}$  state for SiH<sub>2</sub>. The broken and solid spectra for each initial state represent the total flux until 240 fs and 1.2 ps, respectively, after the  $\tilde{A}$ - $\tilde{B}$  photoexcitation. The origin for each curve is shifted for the clarity. The main peaks were assigned to the (0,  $v_2'=0-28$ , 0) levels of the  $\tilde{B}$  state.

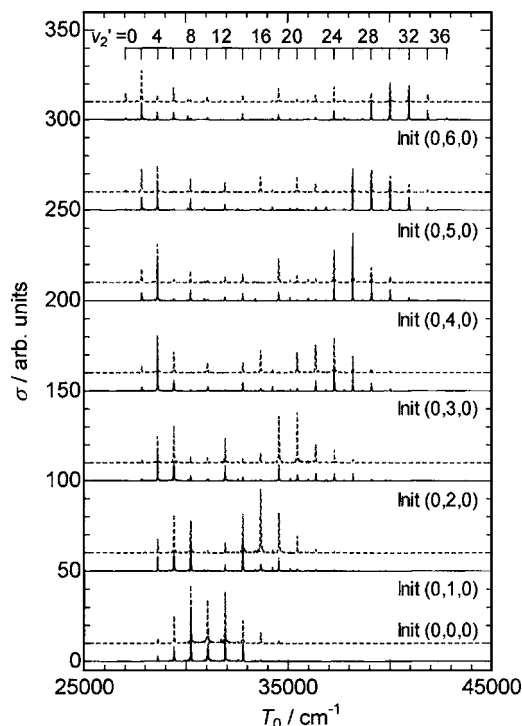


FIG. 4. Same as Fig. 3 but for SiD<sub>2</sub>. The broken and solid spectra for each initial state represent the total flux until 240 fs and 2.4 ps, respectively, after the photoexcitation. The main peaks were assigned to the (0,  $v_2'=0-36$ , 0) levels of the  $\tilde{B}$  state.

we neglected the SiH( $A$ ) + H channel in this calculation with the excitation energy less than 60 000 cm<sup>-1</sup>; the excitation energy represents the energy difference from the vibrational ground level of the  $\tilde{X}$  state in this paper.

Figure 2 shows the photodissociation cross sections ( $\sigma$ ) calculated for SiH<sub>2</sub>, SiHD, and SiD<sub>2</sub> using the (0, 0, 0) vibrational function of the  $\tilde{A}$  state as an initial wave packet. It is clearly seen that the  $\sigma$  spectra consist of a continuous band and a number of sharp peaks. The sharp peaks for SiH<sub>2</sub> and SiD<sub>2</sub> agree well with the vibrational levels of the  $\tilde{B}$  state, whereas the peaks for SiHD seem to be slightly shifted from the vibrational levels of the  $\tilde{B}$  state. The continuous part for SiH<sub>2</sub> and SiD<sub>2</sub> is ca. 10<sup>-16</sup> cm<sup>2</sup> at 30 000 cm<sup>-1</sup> and slightly decreases with the increase of the excitation energy, whereas the  $\sigma$  for SiHD at 50 000 cm<sup>-1</sup> increases by 10<sup>4</sup> times that of 30 000 cm<sup>-1</sup>. This large difference between the feature of SiHD and those of SiH<sub>2</sub> and SiD<sub>2</sub> may originate in the initial wave packet, which is distributed on the PES of the  $\tilde{B}$  state; this will be discussed later.

Figure 3 shows the dependence of  $\sigma$  on the initial wave packet with  $J=0$  of the  $\tilde{A}$  state for SiH<sub>2</sub> and Fig. 4 for SiD<sub>2</sub>. The broken spectrum for each initial state represents the total flux until 240 fs after the photoexcitation, and the solid spectra for SiH<sub>2</sub> and SiD<sub>2</sub> correspond to those until 1.2 and 2.4 ps, respectively. The peaks in the photodissociation spectra correspond to the (0,  $v_2'=\text{even}$ , 0) levels of the  $\tilde{B}$  state. In addition, the very weak lines, which are not assigned in the figures, are attributable to the (1,  $v_2'$ , 0) levels. To investigate the dissociation mechanism, the photodissociation spectra were compared with the photoabsorption spectra calculated

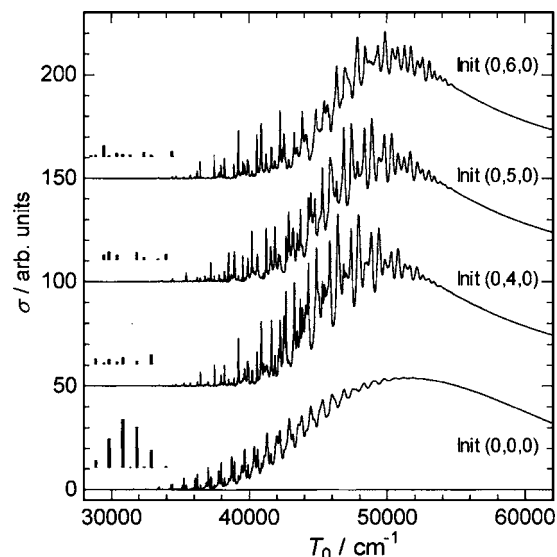


FIG. 5. Same as Fig. 3 but for SiHD; the line spectra are also shown, which represent the photoabsorption based on the FC principle. The curves for each initial state represent the total flux until 240 fs after the photoexcitation.

from Einstein's  $B$  coefficients and the FCFs for the  $\tilde{A}-\tilde{B}$  system; the necessary data were summarized in an EPAPS document.<sup>21</sup> The broken spectra, which mainly consist of the faster component, were found to be almost reproduced by the photoabsorption spectra for the  $\tilde{A}-\tilde{B}$  excitation; the latter spectra are not shown in Figs. 3 and 4. This agreement means that the excitation process is a FC-type and that the dissociation rate is nearly independent of the vibrational levels of the upper state. Nevertheless, the solid spectra, which mainly consist of the slower component, were found to concentrate in a fewer peaks. It may be concluded that the faster component from SiH<sub>2</sub> and SiD<sub>2</sub> mainly corresponds to the direct process, whereas the slower component reflects indirect mechanisms such as postcollision interactions. The dependence of  $\sigma$  on the initial vibrational level with  $J=1$  of the  $\tilde{A}$  state shows very similar profile to that for  $J=0$  except that the peaks correspond to the  $(0, v_2''=\text{odd}, 0)$  levels of the  $\tilde{B}$  state.

Figure 5 shows the dependence of  $\sigma$  on the initial wave packet with  $J=0$  of the  $\tilde{A}$  state for SiHD. The spectrum for each initial wave packet represents the total flux until 240 fs after the photoexcitation. There is no contribution to the flux after 240 fs, i.e., HD is produced from SiHD only via the faster component. These spectra consist of a number of sharp peaks at lower photon energy region, and then the vibrational structure is obscured by a continuous band with the increase of photon energy; the continuous band seems to be continued above 70 000  $\text{cm}^{-1}$ . Nevertheless, we do not discuss the region above 65 000  $\text{cm}^{-1}$  because the SiH(A)+H dissociation, which is not considered in this study, may open. The peaks, which are further complicated than those for SiH<sub>2</sub> and SiD<sub>2</sub>, seem to be shifted ca. 60  $\text{cm}^{-1}$  each other depending on the initial wave packet; we failed to assign these peaks because of strong vibrational coupling. For comparison, the photoabsorption spectrum from each vibrational level of the  $\tilde{A}$  state

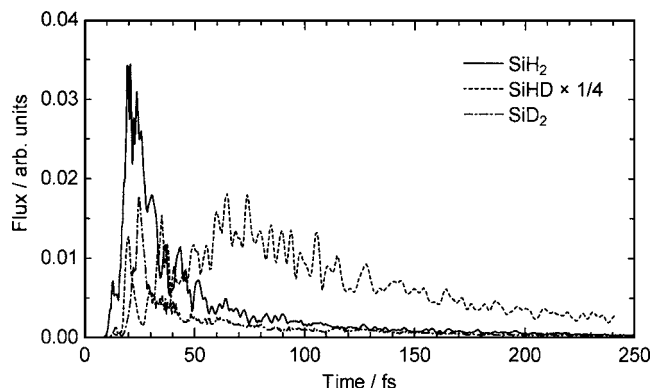


FIG. 6. Population flux of the  $J=0$  wave packet for SiH<sub>2</sub>, SiHD, and SiD<sub>2</sub> leaving the computational grid as a function of time, taken at  $R=3.7$  Å. The initial wave packet is for the  $(0,0,0)$  vibrational function of the  $\tilde{A}$  state.

was calculated from Einstein's  $B$  coefficients and the FCFs for the  $\tilde{A}-\tilde{B}$  system. The obtained photoabsorption spectrum, which clearly reveals a FC envelope, is shown as the line spectrum at the left side for each photodissociation spectrum in Fig. 5. Both the profile and the transition energy of the photodissociation spectrum from the  $(0,0,0)$  initial wave packet are very different from the corresponding photoabsorption spectrum. Although the line spectra from the  $(0, v_2''=4-6, 0)$  levels are rather weak because their FC sums up to the 80th level of the  $\tilde{B}$  state are 0.4–0.5 against the sum

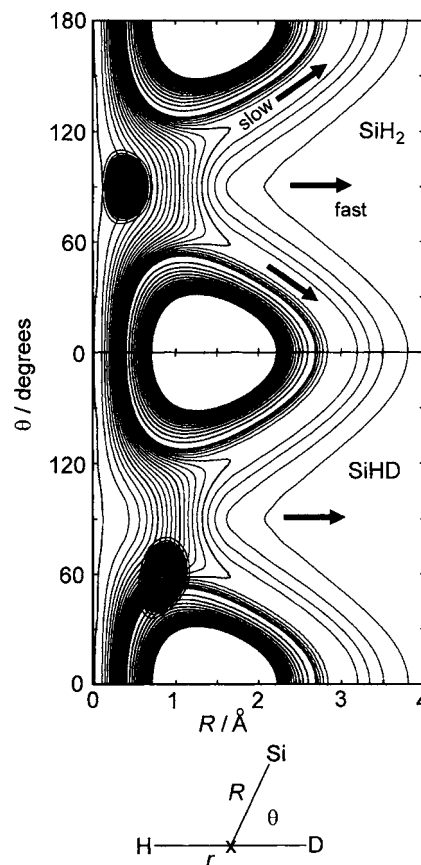


FIG. 7. The  $(0,0,0)$  initial wave packet for SiH<sub>2</sub> and SiHD on the PES of the  $\tilde{B}$  state;  $r$  is fixed at the equilibrium length of 1.47 Å, and for SiHD the H atom is at  $\theta=180^\circ$  and the D atom at  $\theta=0^\circ$ ; the Jacobi coordinate for SiHD is shown at the bottom for clarity.

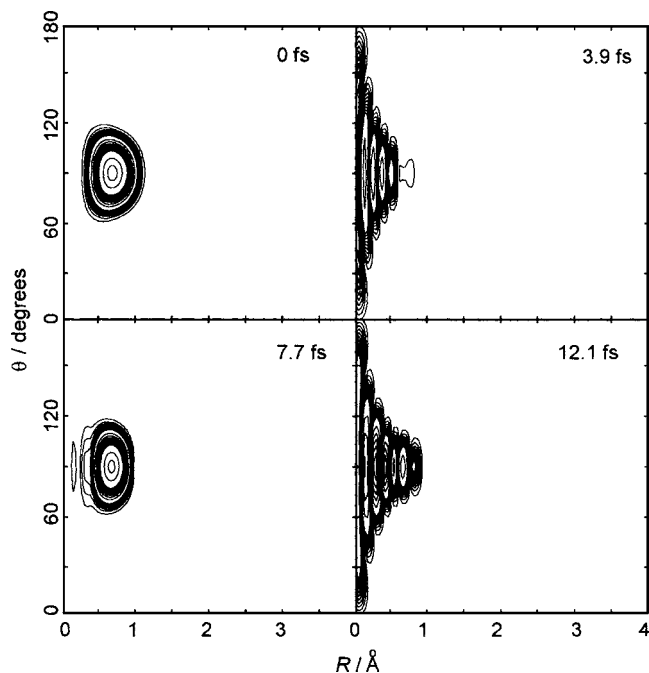


FIG. 8. The wave packet propagation of the (0,0,0) initial wave packet for the  $\tilde{A}$  state of SiH<sub>2</sub>.

of 0.99 for the (0,0,0) level, we have evidently concluded that the dissociation of SiHD is no FC type. The dissociation of SiHD despite of a faster process until 240 fs seems to be very different from the faster components for SiH<sub>2</sub> and SiD<sub>2</sub>, which are FC types.

The lifetime of the  $\tilde{B}$  state is shown in Fig. 6, which presents the flux leaving the computational grid as a function of time using the (0,0,0) initial wave packet for each species. The spectra show heavily fluctuating structures. The first small peak appears at 13–14 fs, which corresponds to a half period of 1200–1300 cm<sup>-1</sup> for the vibrational frequencies. The second intense peaks for SiH<sub>2</sub>, SiHD, and SiD<sub>2</sub> appear at ca. 18, 20, and 25 fs, respectively. The vibrational frequencies of the (0,2,0) levels for SiH<sub>2</sub>, SiHD, and SiD<sub>2</sub> correspond to half periods of ca. 16, 18, and 22 fs, respectively. Therefore, the first peak probably corresponds to a direct dissociation, which seems to be very weak. We reported the fluorescence lifetimes calculated for the  $\tilde{B}$  state of SiH<sub>2</sub> and SiD<sub>2</sub> neglecting the dissociation process.<sup>9</sup> However, even the lifetime for the vibrational ground level seems to be shortened via the predissociation.

Figure 7 shows the PES of the  $\tilde{B}$  state and the (0,0,0) wave function of the  $\tilde{A}$  state for SiH<sub>2</sub> and SiHD; for SiHD the D atom is at  $\theta=0^\circ$  and the H atom is at  $\theta=180^\circ$ . It is clearly seen that the center of the wave function of SiH<sub>2</sub> is around  $\theta=90^\circ$ , whereas that for SiHD is sifted to the D atom. Moreover, the transition moment with  $R$  fixed at 0.8 Å, which has a minimum of 0.3 a.u. at  $\theta=90^\circ$ , increases with the decrease in  $\theta$  and reaches a maximum of 0.6 around  $\theta=50^\circ$ ; the dissociation of SiHD, which deviates from the FC principle, is partly caused by the large dependence of the transition moment on  $\theta$ . The arrows show the dissociation path on the valley of PES. The (0,0,0) vibrational function of

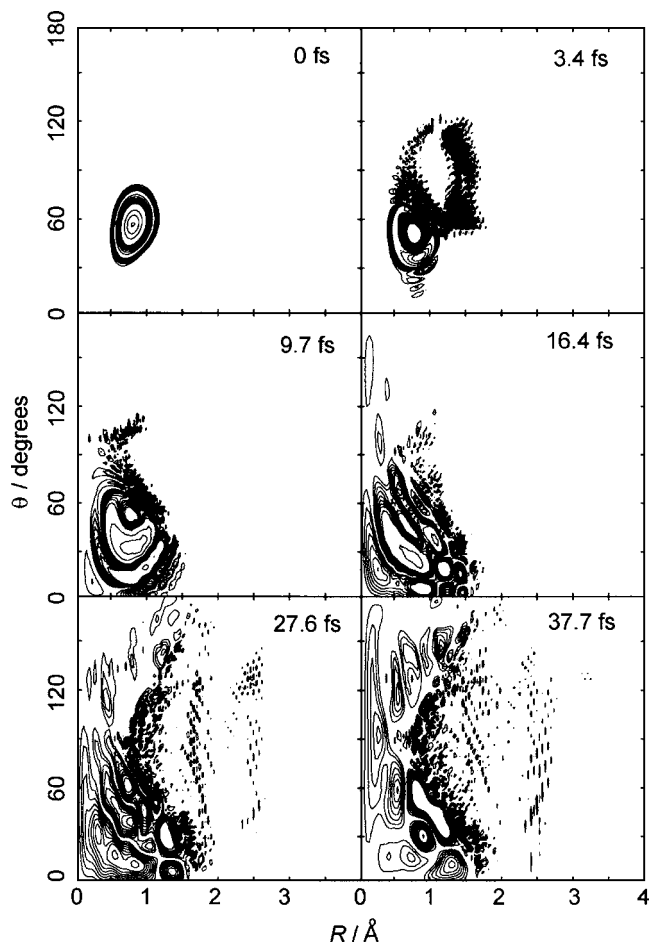


FIG. 9. The wave packet propagation of the (0,0,0) initial wave packet for the  $\tilde{A}$  state of SiHD.

the  $\tilde{A}$  state for SiH<sub>2</sub> is produced around the low energy region according to the FC principle as shown in Fig. 3, while that for SiHD appears around  $\theta=60^\circ$ , which is mainly produced in the higher energy region. For SiH<sub>2</sub> it seems to be very difficult to dissociate directly because the valley to dissociation is very narrow and far from the initial position of the wave packet, and then the initial wave packet is trapped around the local minimum at  $\theta=90^\circ$ . Therefore, the wave packet leaves the computational grids along the valley as shown in Fig. 7 after reflecting on the repulsive wall frequently with slow velocity. This is a Feshbach-type resonance. On the contrary the initial wave packet for SiHD is near the entrance of the valley, and then the wave packet, which mainly has larger kinetic energy, leaves after reflecting on the repulsive wall within shorter time.

Figure 8 shows the propagation of the (0,0,0) initial wave packet for SiH<sub>2</sub> and Fig. 9 for SiHD. The initial wave packet for SiH<sub>2</sub> vibrates around the bottom of the potential well with a period of 8 fs for a long time, and we cannot detect the outgoing flux in this scale because of very low density. On the contrary, the initial wave packet for SiHD spreads rapidly, reflects on the repulsive wall, and then diverges among wide range in angle. We evidently recognize the fluxes that are outgoing periodically. The propagation of the wave packet for SiD<sub>2</sub> is omitted since its appearance is found to be very similar to that for SiH<sub>2</sub>.

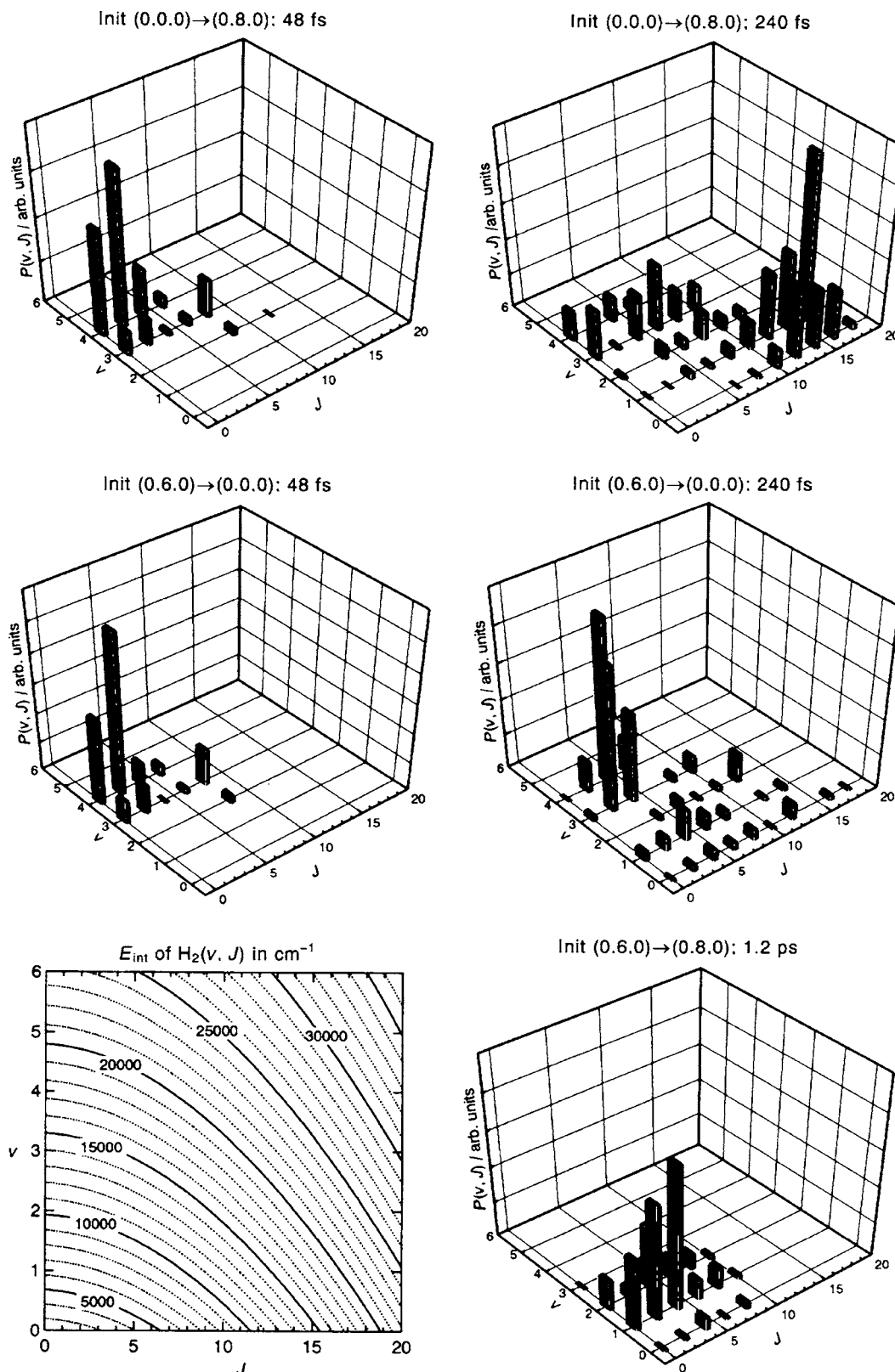


FIG. 10. Rovibrational distribution ( $v, J$ ) of H<sub>2</sub> fragment produced from the  $J=0$  initial wave packet. The two-dimensional (2D) map of  $E_{\text{int}}$  for the ( $v, J$ ) level is shown at the bottom.

The fluxes for SiH<sub>2</sub>, SiHD, and SiD<sub>2</sub>, which leave the computational grid until 240 fs, are 68%, 100%, and 71%, respectively, using the (0,0,0) initial wave function with  $J=0$  of the  $\tilde{A}$  state. The ratio for SiH<sub>2</sub> reaches to 97% until 1.2 ps and that for SiD<sub>2</sub> reaches to 88% until 2.4 ps. When

the vibrational excited functions are adopted as the initial wave packet, the rate of the flux leaving the computational grid increases with the vibrational energy of the initial wave packet for both SiH<sub>2</sub> and SiD<sub>2</sub>. In addition, the dissociation rates using the  $J=1$  initial function become two to three

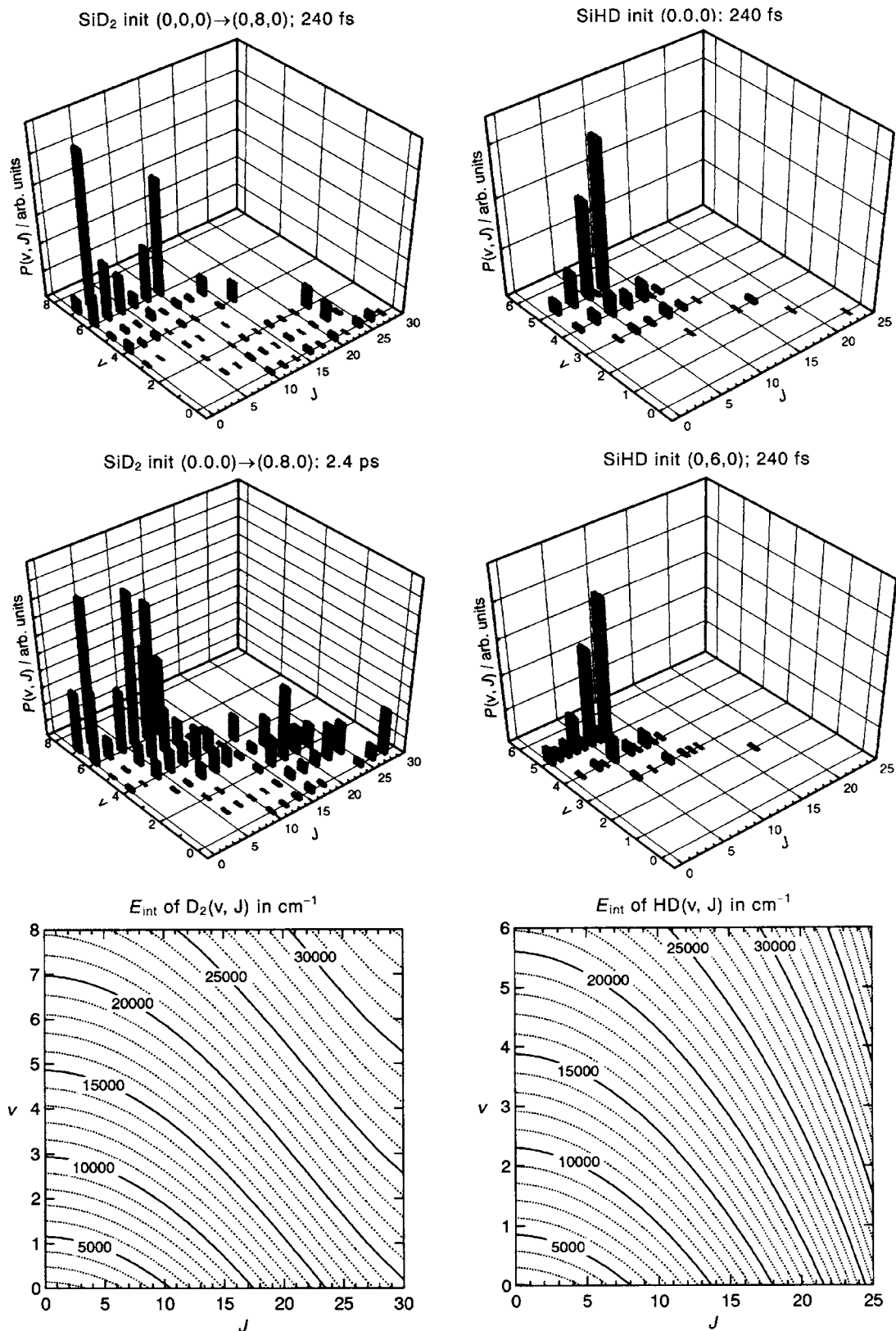


FIG. 11. Rovibrational distribution  $(v, J)$  of  $\text{D}_2$  and HD fragments produced from the  $J=0$  initial wave packet. The 2D map of  $E_{\text{int}}$  for the  $(v, J)$  level is shown at the bottom.

times as much as the rate with  $J=0$  for both  $\text{SiH}_2$  and  $\text{SiD}_2$ . The difference in the rates with  $J=0$  and 1 may be explained by the propagation of the wave packet because the energy difference is only a few  $\text{cm}^{-1}$ . Therefore, the observation<sup>8</sup> that the dissociation rate of  $\text{SiH}_2$  is larger than that of  $\text{SiD}_2$

may be originated in the mass difference rather than tunneling effects. The fast rate in the dissociation of  $\text{SiHD}$  is probably attributed to the profile of the vibrational wave functions. Even in the time-dependent formulation<sup>22</sup> there is the possibility for dynamical behavior, including Feshbach

resonances. It may be concluded that the  $\tilde{B}$  state dissociates to the Si(<sup>1</sup>D)+H<sub>2</sub> product mainly via the indirect process, including Feshbach resonances, as shown in Figs. 7 and 8. In the case illustrated, there is a resonance between the dissociation path and bending motions.<sup>23</sup>

### C. Internal distribution of H<sub>2</sub>/HD/D<sub>2</sub> products

The rovibrational distributions of the H<sub>2</sub> fragment produced by the SiH<sub>2</sub>( $\tilde{B}$ )→Si(D)+H<sub>2</sub> dissociation were calculated by using several initial wave packets. Figure 10 shows the results from the initial wave packet with  $J=0$ ; the internal energy  $E_{\text{int}}$  of H<sub>2</sub>( $v, J$ ) is also shown at the bottom of Fig. 10. The faster component until 48 fs via the (0,8,0) level of the  $\tilde{B}$  state from the (0,0,0) initial wave packet has a distribution of vibrationally hot and rotationally cold, whereas the slower component until 240 fs mainly has a distribution of vibrationally cold and rotationally hot as shown at the top of Fig. 10. The  $E_{\text{int}}$  of the main distributions are rather sharp and correspond to ca. 18 000 cm<sup>-1</sup> against the available energy of 23 600 cm<sup>-1</sup>. For the (0,0,0) initial wave packet, the similar features are obtained for the flux via the (0,  $v_2=4-12$ , 0) levels of the  $\tilde{B}$  state. The results are true for flux via the (0,0,0) levels of the  $\tilde{B}$  state when the higher vibrational functions are adopted as the initial wave packet, as shown at the middle of Fig. 10. The upper limit of  $E_{\text{int}}$  is estimated to be ca. 18 000 cm<sup>-1</sup> against the available energy of 19 200 cm<sup>-1</sup>. The  $E_{\text{int}}$  of the main distribution is found to occupy the greater part of the available energy probably because of the large change in the distance of H–H and the mass ratio of H<sub>2</sub> to Si. However, the internally cold H<sub>2</sub> appears as the slower component of the flux until 1.2 ps via the (0,8,0) levels of the  $\tilde{B}$  state when the (0,6,0) wave function is adopted as the initial wave packet (right bottom of Fig. 10). In addition, the distribution from the (0,6,0) initial wave packet is broader than that from the (0,0,0) initial wave packet. These features indicate strong coupling between the internal and translational modes of the product channels.

Figure 11 shows the results for D<sub>2</sub> and HD with  $J=0$ . For D<sub>2</sub> the faster component until 240 fs via the (0,8,0) level of the  $\tilde{B}$  state from the (0,0,0) initial wave packet has a distribution of vibrationally hot and rotationally cold, whereas the slower component includes a distribution of vibrationally cold and rotationally hot. The similar feature is obtained for the flux via the (0,  $v_2=4-14$ , 0) levels of the  $\tilde{B}$  state. The main distributions until 240 fs are rather sharp with  $E_{\text{int}}$  of 18 000–20 000 cm<sup>-1</sup> against the available energy of 22 200 cm<sup>-1</sup>. These results are nearly equal to those for SiH<sub>2</sub>. The same is true for the flux via lower vibrational levels from the (0,  $v_2$ , 0) initial wave packet with  $v_2=1, 5, 6$  despite of rather broader distribution. Nevertheless, we did not find the internally cold distribution for the flux via higher vibrational levels of the  $\tilde{B}$  state, even if higher vibrational functions were used as the initial wave packet. When the initial wave packets with  $J=1$  were used, the distributions were very similar to those for the initial wave packets with  $J=0$ . For SiHD the rovibrational distributions of HD fragment are mainly vibrationally hot and rotationally

cold and similar to those for the faster component of SiH<sub>2</sub> and SiD<sub>2</sub>. The  $E_{\text{int}}$  of the distributions are ca. 18 000–19 000 cm<sup>-1</sup> against the available energy of 27 000–42 000 cm<sup>-1</sup>. The  $E_{\text{int}}$  of H<sub>2</sub> fragment produced from the SiH<sub>2</sub>( $\tilde{B}$ )→H<sub>2</sub>+Si dissociation seems to be insensitive to the available energy.

### IV. SUMMARY

To study the photodissociation process SiH<sub>2</sub>( $\tilde{A}$ )→SiH<sub>2</sub>( $\tilde{B}$ )→Si(<sup>1</sup>D)+H<sub>2</sub>, the wave packet propagation calculations were applied to the PES of the  $\tilde{B}$  state. The autocorrelation function was computed by numerically integrating the product of the initial wave packet and the evolving wave packet at each time step; the vibrational functions for the  $\tilde{A}$  state were used as the initial wave packet. Total photodissociation  $\sigma$  as a function of the excitation energy was calculated as the Fourier transform of the autocorrelation function. The photoabsorption spectra calculated for SiH<sub>2</sub> consist of a continuous band and a number of sharp peaks. The dependence of the  $\sigma$  for SiD<sub>2</sub> on the photon energy is similar to that for SiH<sub>2</sub>, whereas that for SiHD is very different from SiH<sub>2</sub>. The fluxes for SiH<sub>2</sub> and SiD<sub>2</sub> consist of the faster and slower components, whereas only the faster component is produced from SiHD. The faster component is vibrationally hot and rotationally cold, while the main part of the slower component is vibrationally cold and rotationally hot. The results of this study show large isotope effects between the dissociation of SiH<sub>2</sub>/SiD<sub>2</sub> and that of SiHD, which have not been found experimentally yet. These isotope effects are originated in the feature of PESs for the  $\tilde{A}$  and  $\tilde{B}$  states and the difference in the vibrational wave functions between three isotopomers.

### ACKNOWLEDGMENT

The computation was mainly carried out using the computer facilities at the Research Center for Computational Science of The Okazaki National Institutes.

- <sup>1</sup>J. W. Thoman, Jr., J. I. Steinfeld, R. I. McKay, and A. E. W. Knight, *J. Chem. Phys.* **86**, 5906 (1987).
- <sup>2</sup>C. M. Van Zoeren, Y. J. W. Thoman, Jr., J. I. Steinfeld, and M. W. Rainbird, *J. Phys. Chem.* **92**, 9 (1987).
- <sup>3</sup>J. S. Francisco, R. Barnes, and J. W. Thoman, Jr., *J. Chem. Phys.* **88**, 2334 (1988).
- <sup>4</sup>R. I. McKay, A. S. Uichanco, A. J. Bradley, J. R. Holdsworth, J. S. Francisco, J. I. Steinfeld, and A. E. W. Knight, *J. Chem. Phys.* **95**, 1688 (1991).
- <sup>5</sup>M. Fukushima, S. Mayama, and K. Obi, *J. Chem. Phys.* **96**, 44 (1992).
- <sup>6</sup>M. Fukushima and K. Obi, *J. Chem. Phys.* **100**, 6221 (1994).
- <sup>7</sup>M. Nakajima, A. Kawai, M. Fukushima, and K. Obi, *Chem. Phys. Lett.* **364**, 99 (2002).
- <sup>8</sup>Y. Muramoto, H. Ishikawa, and N. Mikami, *J. Chem. Phys.* **122**, 154302 (2005).
- <sup>9</sup>I. Tokue, K. Yamasaki, and S. Nanbu, *J. Chem. Phys.* **122**, 144307 (2005).
- <sup>10</sup>D. E. Woon and T. H. Dunning, Jr., *J. Chem. Phys.* **98**, 1358 (1993) and references cited therein.
- <sup>11</sup>J. V. Lill, G. A. Parker, and J. C. Light, *Chem. Phys. Lett.* **89**, 483 (1982).

- <sup>12</sup>D. T. Colbert and W. H. Miller, *J. Chem. Phys.* **96**, 1982 (1992).
- <sup>13</sup>E. M. Goldfield and S. K. Gray, *Comput. Phys. Commun.* **98**, 1 (1998).
- <sup>14</sup>C.-Y. Yang and S. K. Gray, *J. Chem. Phys.* **107**, 7773 (1997).
- <sup>15</sup>R. B. Lehoucq, K. Maschhoff, D. C. Sorensen, and C. Yang, ARPACK, Rice University, Houston, 1997; see the ARPACK homepage at <http://www.caam.rice.edu/software/ARPACK/>
- <sup>16</sup>S. K. Gray and G. G. Balint-Kurti, *J. Chem. Phys.* **108**, 950 (1998).
- <sup>17</sup>S. Nanbu and M. S. Johnson, *J. Phys. Chem. A* **108**, 8905 (2004).
- <sup>18</sup>R. Chen and H. Guo, *Comput. Phys. Commun.* **119**, 19 (1999).
- <sup>19</sup>L. Fredin, R. H. Hauge, Z. H. Kafafi, and J. L. Margrave, *J. Chem. Phys.* **82**, 3542 (1985).
- <sup>20</sup>W. Gabriel, P. Rosmus, K. Yamashita, K. Morokuma, and P. Palmieri, *Chem. Phys.* **174**, 45 (1993).
- <sup>21</sup>EPAPS Document No. E-JCPSA6-122-312515 attached to Ref. 9.
- <sup>22</sup>M. D. Feit, J. A. Fleck, and A. Steiger, *J. Comput. Phys.* **47**, 412 (1982).
- <sup>23</sup>C. Leforestier, F. LeQuere, K. Yamashita, and K. Morokuma, *J. Chem. Phys.* **101**, 3806 (1994).